Journal of Environmental Management 324 (2022) 116263

Contents lists available at ScienceDirect

Journal of Environmental Management

journal homepage: www.elsevier.com/locate/jenvman

Research article

Does city-water layout matter? Comparing the cooling effects of water bodies across 34 Chinese megacities

Zhi Cai [a], Jean-Michel Guldmann [b], Yan Tang [a,*], Guifeng Han [c]

[a] School of Architecture, Tsinghua University, Beijing, 100084, China
[b] Department of City and Regional Planning, The Ohio State University, 275 West Woodruff Avenue, Columbus, OH, 43210, USA
[c] School of Architecture and Urban Planning, Chongqing University, Chongqing, 400045, China

ARTICLE INFO

Keywords:
Thermal environment
Cooling effect
Waterbodies
Land surface temperature
Climate regions

ABSTRACT

As most cities are located around or near waterbodies, it is essential to assess the thermal effect of these waterbodies. This research focuses on 34 Chinese megacities as case studies to examine the spatial relationship between city-water layout and the thermal effect of waterbodies. Landsat-8 remote-sensing images acquired around noontime in summer were used to retrieve land surface temperatures (LST) and classify land cover. The results show that there are three types of city-water layout. For most cities, waterbodies have a cooling effect, and their mean cooling distance (ΔL_{max}) ranges from 431 m to 1350 m, with the maximum temperature difference (ΔT_{max}) ranging from - 2.21 °C to 7.83 °C. The cooling effect of waterbodies is also influenced by their spatial distribution, size, location, and background climate regions. The larger the percentage or area of waterbodies in a city, the shorter ΔL_{max} and the bigger ΔT_{max}. Waterbodies have the longest ΔL_{max} and the smallest ΔT_{max} when they are dispersed within the city, whereas they have the shortest ΔL_{max} and the largest ΔT_{max} when they are flowing through the city. The results suggest that the thermal effects of waterbodies should be seriously considered by urban planners to improve the urban microclimate.

1. Introduction

Air temperatures in urban areas are higher than in their surrounding rural areas. This phenomenon is known as the urban heat island (UHI) and was first discovered by Howard in London. Later, scholars uncovered several types of UHI, such as boundary-layer heat islands and surface urban heat islands (SUHI) (Oke et al., 2017). The UHI can lead to more energy consumption in the summer due to rising cooling needs (Shen et al., 2013; Wilson, 2013; Almeida et al., 2021; Singh and Sharston, 2022). Combined with the trend of frequent heatwaves, the UHI exposes vulnerable people (e.g., elders, patients, and children) to health risk (Cai et al., 2019; Zhao et al., 2018; Van Hoof et al., 2017; Zhang et al., 2019), increasing their morbidity and mortality (Rydin et al., 2012; Zhang et al., 2019; Mora et al., 2017; Yang et al., 2019). Because of global warming and rapid urbanization, global average surface temperatures will continue to rise (Lindsey, 2014; Sippel et al., 2020), and 68% of the world population will live in urban areas by 2050 (United Nations, 2019), leading to even greater adverse effects of the thermal environment on urban residents. Therefore, it is urgent for cities to adapt to global warming and mitigate the UHI (Klok and Kluck, 2018; Manoli et al., 2019).

One of the mitigation methods is to optimize the urban spatial form by expanding green spaces (Masoudi et al., 2019), waterbodies, and wetlands (Ghosh and Das, 2018; Sun et al., 2012). Due to their higher heat capacity, waterbodies play a more active role in cooling cities than green spaces and wetlands (Xue et al., 2019; Sun et al., 2012; Jiang et al., 2021). While receiving the same amount of solar radiation, waterbodies have their temperatures rise more slowly than paved and building surfaces, making them cold islands during daytime (Klok and Kluck, 2018), especially in the morning. In order to study the cooling effects of waterbodies, scholars have used different methods, such as remote-sensing monitoring, in-situ measurements, and statistical modeling. These studies show that waterbodies have a strong cooling effect on their surrounding areas because of evapotranspiration (Fig. 1), especially downwind (Cai et al., 2018; Du et al., 2016; Park et al., 2019; Moyer and Hawkins, 2017; Syafii et al., 2017). For example, Park et al. (2019) using moving survey thermometer and weater station data, find that the cooling distance of a small river (with an average width of 8 m) can reach 32.7 m, with a cooling intensity of 0.46 °C in the afternoon. Over all, the cooling distance of waterbodies ranges from 12 m to several

* Corresponding author.
E-mail addresses: czhi0911@gmail.com (Z. Cai), guldmann.1@osu.edu (J.-M. Guldmann), yantang@mail.tsinghua.edu.cn (Y. Tang), hangf@cqu.edu.cn (G. Han).

https://doi.org/10.1016/j.jenvman.2022.116263
Received 31 December 2021; Received in revised form 22 May 2022; Accepted 10 September 2022
Available online 24 September 2022
0301-4797/© 2022 Elsevier Ltd. All rights reserved.

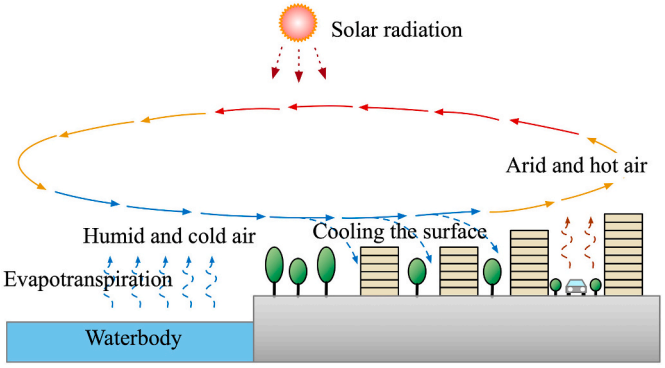


Fig. 1. Water/land breeze system for an urban area in summer noontime.

kilometers, reducing the surrounding temperatures by several degrees (Du et al., 2016; Park et al., 2019; Tsai et al., 2017; Adams and Smith, 2014; Qiu et al., 2021).

Studies also find that the cooling effect of waterbodies is influenced by several factors, such as their size and geometry (Sun and Chen, 2012; Zhu et al., 2011; Gunawardena et al., 2017; Theeuwes et al., 2013; Hathway and Sharples, 2012; Wang et al., 2019). For example, broad and regular waterbodies have a stronger cooling effect than narrow and irregular ones (Zhu et al., 2011; Gunawardena et al., 2017; Wu et al., 2019). Urban canopy-layer conditions and the urban spatial form are the other factors that affect cooling effects (Hathway and Sharples, 2012; Wang and Ouyang, 2021), and studies indicate that open streets and city squares increase this cooling effect, whereas tall buildings or high walls decrease it (Hathway and Sharples, 2012).

However, it should be noted that, besides waterbody characteristics and urban canopy-layer conditions, other factors (e.g. city-water layout, local climate zone) can also influence the cooling effects of waterbodies. For example, cities display large variations in waterbody spatial distribution and coverage, which creates varying city-water landscapes, such as coastal cities, river-side cities, lake-side cities, and even desert cities, with significant differences in their urban thermal environment (Lin et al., 2020). Moreover, depending upon the dry-wet climate regions where the cities are located, waterbodies may also have different thermal effects, and even warming effects (Steeneveld et al., 2014; Bande et al., 2019). The above factors are difficult to uncover in single-city studies and require comprehensive multiple-city comparisons. Therefore, 34 Chinese megacities, with various city-water layouts and locations in different dry-wet climate regions, were selected to answer the following questions:

a. What is the cooling effect of waterbodies across different cities with various city-water layouts?
b. How does the dry-wet regional climate impact waterbody cooling effects?

2. Data and methods

2.1. Data sources and pre-processing

2.1.1. Study area and data sources

The 34 Chinese cities' locations are depicted in Fig. 2, including 26 provincial capital cities, 4 province-level cities (Beijing, Tianjin, Shanghai and Chongqing), and 4 typical coastal or lakeside municipal cities (Xiamen, Ningbo, Qingdao, Wuxi). They are located in four dry-wet climate regions, based on their humidity index: arid, semi-arid, semi-humid and humid regions. The radius of these cities ranges from 3 km (Lanzhou) to 18 km (Shanghai). Since the strongest cooling effect of waterbodies takes place in summer daytime (Chun and Guldmann,



Fig. 2. Spatial distribution of the selected cities in different dry-wet climate regions.

2018; Sun et al., 2019), Landsat-8 cloud-free remote-sensing (RS) images (Collection 2 Level-1, 30 m spatial resolution) over this study cities and acquired around 10:30 a.m. (local solar time) in summer were downloaded from the USGS website (https://earthexplorer.usgs.gov/) (Appendix 1). Google map layers with super-high resolution (2 m spatial resolution) of the study areas were clipped from Google Earth Pro.

2.1.2. Pre-processing

The different bands of Landsat-8 RS images were used to calculate the Normalized Difference Vegetation Index (NDVI), the Normalized Difference Built-up Index (NDBI) and the Modified Normalized Difference Water Index (MNDWI) (Xu, 2008). All data were imported into ArcGIS Pro software (version 2.5.1) for georeferencing and study area clipping. In order to georeference the Google map layers using Landsat 8 Collection 2 level-1 data (WGS 84 Coordinate System) as a reference image, at least 12 evenly distribution ground control points were selected for each city. The root mean squared error (RMSE) value between Google layers and RS images is smaller than 0.5 pixel.

2.2. Methods

The following four steps are involved: 1) identifying urban and water boundaries, 2) setting buffer zones, 3) setting the spatial scale and processing data, 4) assessing the cooling effects of waterbodies and spatial analysis (Fig. 3).

2.2.1. Identifying the boundaries of urban and waterbodies

Landsat-8 remote-sensing images and Google map layers are used to identify urban boundaries and waterbodies. Usually, NDBI can characterize built-up areas and MNDWI can be used to classify waterbodies (Xu, 2007; Wu et al., 2020). However, land surfaces with little green coverage (e.g., soil, sand) have also high NDBI values and may be interpreted as built-up areas. Also, some land covers or features like building shadows may be confused with waterbodies. In order to avoid misclassification, the threshold values of NDBI > 0 and MNDWI > 0.05 are set by visual interpretation. Google map layers are also used to manually corrects urban and waterbody boundaries. Small ponds and narrow rivers with width below 30 m are ignored because of the spatial limitation of RS images ($\geq$ 30 m).

2.2.2. Setting buffer zones and identifying city-water layout

In order to capture the size of a city and its waterbodies, the geometric center of a city is set as the origin, and then the distances from this center to all grid cells on the urban boundaries are computed. The mean distance is then taken as the city radius (R). A buffer zone, with a width equal to 0.4 R is delineated outside of and adjacent to the urban boundary (Fig. 3c). This buffer is assumed to represent the surrounding rural areas, with a size close to the urban area size (and equal to it if the city were a perfect circle).

The percentage of waterbodies (WP_j), and the types of urban layout and waterbodies distributions (T_k) are used to identify and characterize the city-water layout. WP_j and T_k are defined in Eqs. (1) and (2), respectively:

$$WP_j = \frac{\sum_{i \in j} W_i}{TA_j} * 100\% \quad (\mathrm{j} = \mathrm{U}, \mathrm{R}) \tag{1}$$

$$T_K = \frac{WP_U}{WP_R} \quad (\mathrm{K} = 0, 1) \tag{2}$$

where WP_j is the percentage of waterbodies in the urban ($j = U$, WP_U) or rural ($j = R$, WP_R) area of the city, TA_j is the total urban or rural area, i is a cell located in the urban or rural area, and W_i is the waterbody area in cell i.

If there are only small rivers (width $\leq$ 100 m) flowing through or around the city, then $K = 0$ and $T_0 = 0$, and these cities are characterized as Type I. If there are medium and large river bodies (width >100 m) flowing through or around the city, then $K = 1$. $T_1 > 1$ denotes that the urban area has more waterbodies than the rural area, with waterbodies located throughout the city. These cities are characterized as Type II. $T_1 < 1$ denotes that the urban area has smaller waterbodies than the rural area, with most waterbodies located around the city or with the city located on one side of the waterbodies. These cities are characterized as Type III.

2.2.3. Setting the spatial scale and processing the data

(1) Setting the spatial scale

Several studies have shown that the results of urban spatial analyses are influenced by the spatial scale, particularly in the cases of the urban thermal environment, and the optimal scale varies across different cities (Chun and Guldmann, 2014; Han et al., 2016; Song et al., 2014; Wang et al., 2016). Some studies have also found that urban form indicators display the strongest correlations with LST around a 300-m spatial scale (Du et al., 2016; Dai et al., 2019). In order to cope with multiple bands pixels in 30 m resolution and thermal bands in 100 m resolution, a 300 m $\times$ 300 m grid cell is selected to summarize or average the data (Fig. 3d).

(2) Retrieval of LST

The radiative transfer equation (RTE) method is used to retrieve LST from Landsat-8 TIRS band 10. For more details about this method, see Alvarez-Mendoza et al. (2020), Cai et al. (2021), and Sekertekin and Bonafoni (2020). The retrieved results shows that most citie have a

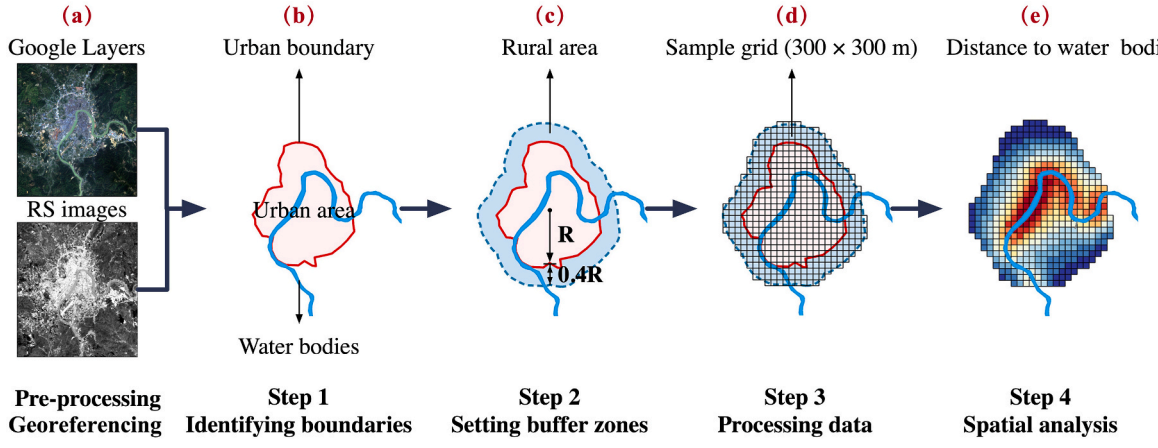


Fig. 3. Processing steps (R represents the radius of the city).

median LST around 40 ℃ (Appendix 2) and are compareable.

2.2.4. Finding the cooling effect of waterbodies and spatial analysis

Previous studies have found that LST displays a rising trend away from waterbodies due to their cooling effect (Du et al., 2016; Sun et al., 2012), and the scatter plots between LST and the distance away from the nearest water body (DW) can be curve-fitted (Fig. 4). Some researchers have manually sought the first turning point of the fitted curve (Du et al., 2016; Sun et al., 2012). However, it is hard to find the turning point when the curve changes smoothly. Therefore, some updated methods have been applied, such as (1) using temperature slope and basin derived from terrain analysis to determine the cooling extent (Lin et al., 2015), or (2) using a logarithmic function to fit scatter plots and get the threshold value (Yang et al., 2020). Some studies have also found that the scatter plots can be fitted as a third-order polynomial function (Cai et al., 2018; Park et al., 2019), where the cooling distance and the temperature difference can be easily found by calculating the first maximum point. The function can be expressed as follows:

$$LST = \mathrm{a} * DW^3 + b*DW^2 + c * DW + d \quad (3)$$

where a, b, c and d are parameters to be estimated. The cooling distance (ΔL_{max}) and the maximum temperature difference (ΔT_{max}) can be identified by seeking the value of DW that sets the derivative of LST to zero (Park et al., 2019; Jaganmohan et al., 2016) (Fig. 4):

$$\Delta L_{max} = \frac{-2b \pm \sqrt{4b^2 - 12ac}}{6a} \quad (4)$$

$$\Delta T_{max} = a*(\Delta L_{max})^3 + b*(\Delta L_{max})^2 + c * \Delta L_{max} \quad (5)$$

3. Results

3.1. Waterbodies in different types of cities

All the case study cities have waterbodies within both urban and and rural areas. Their urban layout and waterbodies distribution can be classified into three types: waterbodies dispersed within the city (Type I), waterbodies flowing through the city (Type II), and waterbodies on one side of the city (Type III) (Fig. 5). Type I cities are all inland cities and almost in the semi-humid zone. Most of Type II cities are inland cities and located in the humid zone. Most of Type III cities are located on one side of a large river, lake, or ocean, and likely located in the humid zone and along the coast.

Cities with different city-water layouts differ in WP. Cities tend to have a higher WP when a river flows through or around it. Fig. 6a shows that WP_U ranges from 0.22% to 15.49%, and the median WP_U increases from Type I cities (1.21%) to Type III cities (2.75%) to Type II cities (5.63%) (Figs. 6a–1). WP_R ranges from 0.49% to 32.82% (Fig. 6b), and the median WP_R increases from Type I cities (1.64%) to Type II cities (2.71%) to Type III cities (16.70%) (Figs. 6b–1). Type I cities have similar WP in their urban and rural areas. However, for Type II and Type III cities, there are big WP differences between urban and rural areas (Fig. 6a and b). Type II cities tend to have more waterbodies than their surrounding rural areas, because of wide rivers flowing through the city and many human-made small lakes within the city. In contrast, Type III cities have fewer waterbodies than their surrounding rural areas, because of large lakes and the ocean located outside urban areas.

3.2. The cooling effect of waterbodies across the different types of cities

DW has a significant positive relationship with LST in 31 cities, as the Pearson correlation coefficient ranges from 0.043** (HB) to 0.417** (LZ), with the strongest coefficients in Type II cities (Fig. 7a). Thus, in those cities, LST rises with DW. The scatter plots between LST and DW show that the rising trend takes place within a limited distance, beyond which LST becomes stable and is no longer correlated with DW (Fig. 4b). This confirms that waterbodies have a cooling effect on the surrounding area within a limited distance.

ΔL_{max} and ΔT_{max} also show that the cooling effect of waterbodies varies across cities. ΔL_{max} ranges from 431.6 m (HZ) to 1350 m (XM) (Fig. 8a), and the median ΔL_{max} decreases from Type I cities (1131.1 m) to Type III cities (908.9 m) to Type II cities (896.5 m) (Figs. 8a–1). ΔT_{max} ranges from - 2.21 °C (UQ) to 7.83 °C (WH) (Fig. 8b), and the median ΔT_{max} decreases from Type II cities (3.81 °C) to Type III cities (2.52 °C) to Type I cities (1.98 °C) (Figs. 8b–1).

Further analyses show that WP_U has a significant negative relationship with ΔL_{max} (−0.447**) and a significant positive relationship with ΔT_{max} (0.629**), underscoring that the larger the percentage of waterbodies in a city, the bigger the temperature difference, but the shorter the cooling distance.

3.3. Waterbody size and its cooling effect

Previous studies have found that the cooling effect of waterbodies is influenced by their size (Sun et al., 2012; Zhu et al., 2011; Hathway and Sharples, 2012; Wang et al., 2019). In order to further assess this influence, waterbodies are classified into three categories (river, lake, ocean) and seven classes (small river, medium river, large river, small lake, medium lake, large lake, ocean) according to their width or area (Table 1). The results show that larger waterbodies tend to have a stronger cooling effect than smaller ones. The median ΔL_{max} decreases in the following order: large lake (904.4 m), large river (735.2 m), small river (668.7 m), small lake (577.5 m), medium lake (559.7 m), ocean (559.4 m) and medium river (528.9 m) (Fig. 9a). The median ΔT_{max}

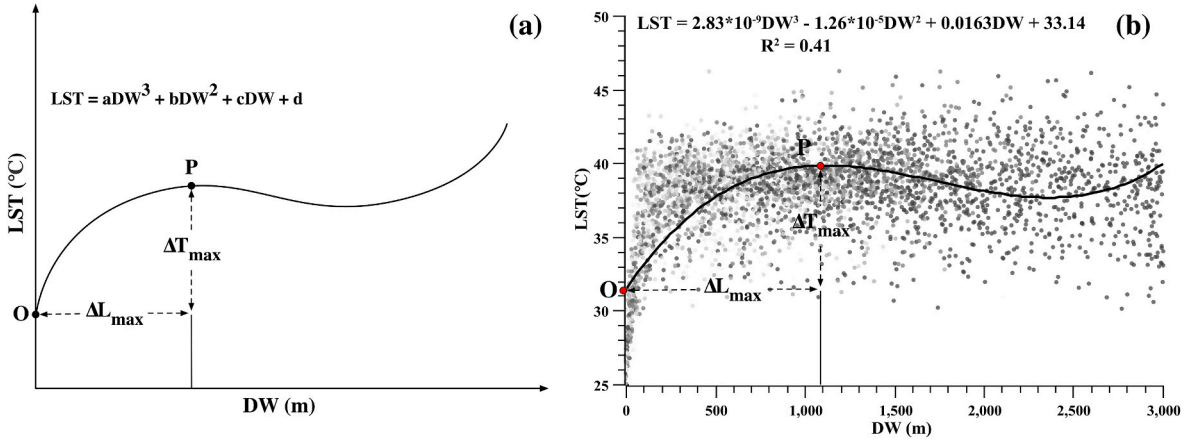


Fig. 4. (a) Conceptual third-order polynomial curve; (b) Scatter plots between LST and DW (Lanzhou urban area).

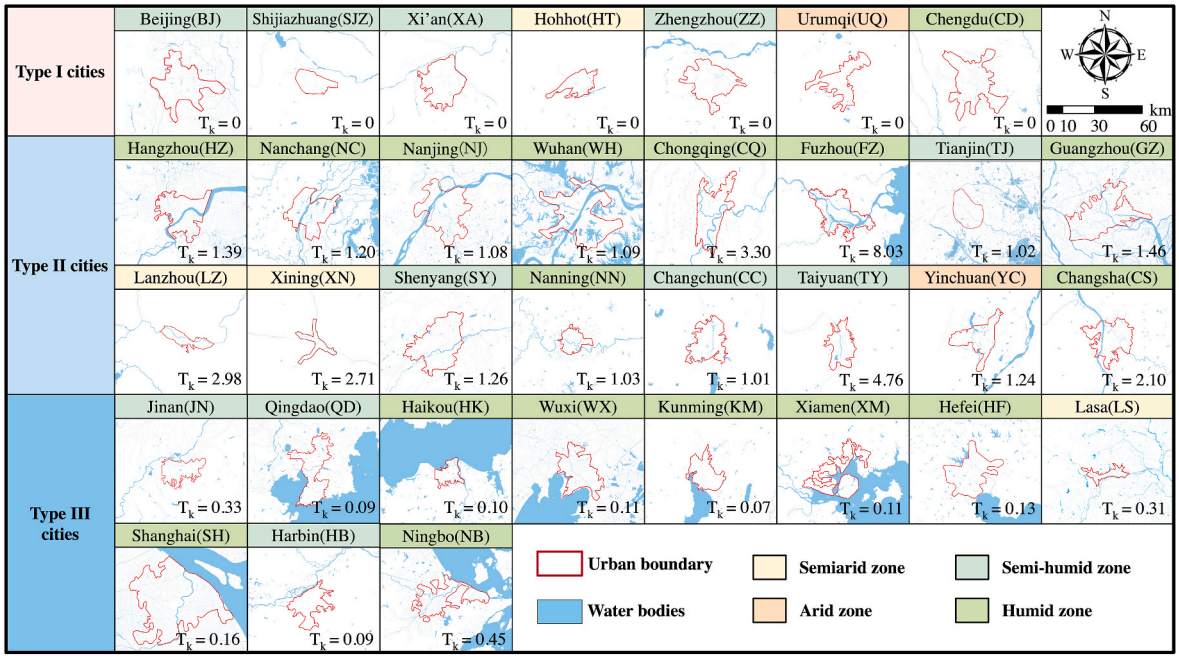


Fig. 5. City-water layouts for 34 cities and 4 dry-wet climate regions (See Appendix 3 for the aerial images of those cities).

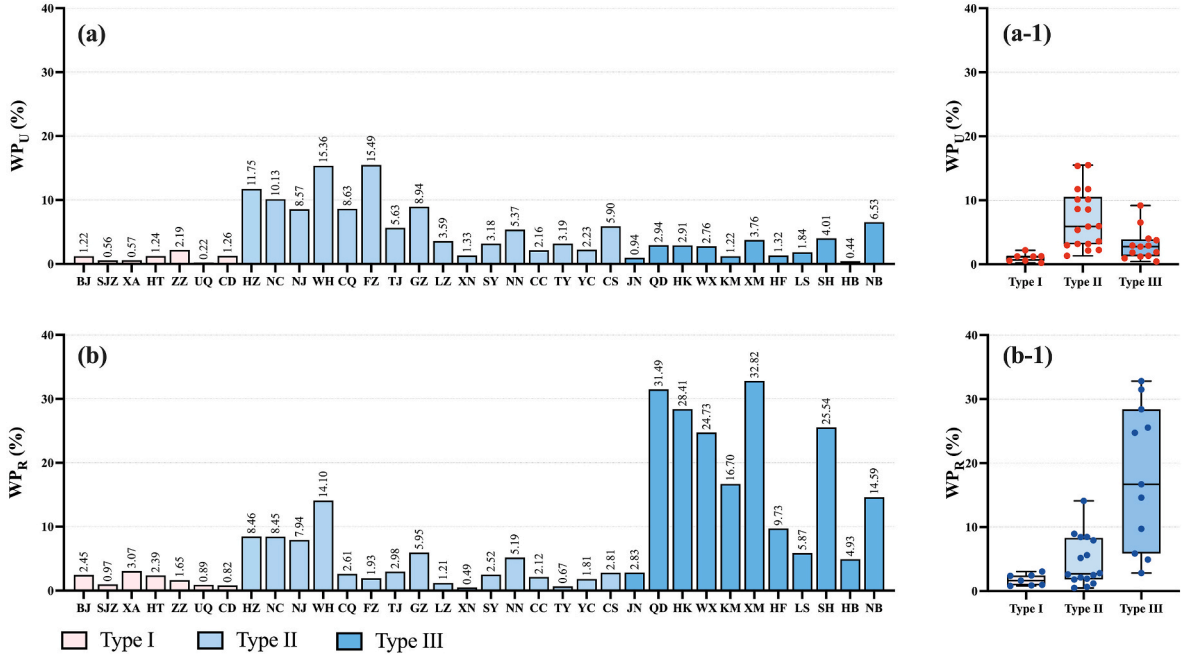


Fig. 6. Distribution of WP_U (a) and WP_R (b) across the 34 cities; Box plots of WP across different city-water layout types in urban areas (a-1) and rural areas (b-1).

decreases as follows: large river (7.7 °C), ocean (6.54 °C), large lake (6.25 °C), medium lake (5.5 °C), medium river (5.0 °C), small lake (4.5 °C) and small river (3.0 °C) (Fig. 9b).

3.4. The cooling effect of waterbodies across different dry-wet climate zones

The median ΔL_{max} for cities in different dry-wet climate regions decreases as follows: semiarid zone (1023.62 m), semi-humid zone (1008.11 m), arid zone (1001.99 m) and humid zone (874.56 m) (Fig. 10a). The median ΔT_{max} in urban areas decreases as follows: humid zone (3.75 °C), semiarid zone (2.54 °C), semi-humid zone (1.98 °C) and arid zone (1.53 °C) (Fig. 10b). In summer daytime, a waterbody has strong evaporation. The air in the humid zone has higher humidity than in the arid zone. Moist air is expected to have a higher heat capacity and can reduce the efficiency of water evapotranspiration (Ampatzidis and Kershaw, 2020), which produce a large ΔT_{max} and a shorter cooling distance.

3.5. The cooling effect of waterbodies in urban and rural areas

Compared to urban areas, DW in rural areas has weaker correlations with LST in most of Type I and Type II cities (Fig. 7a and b), which suggests that waterbodies have a weaker cooling effect in rural areas.

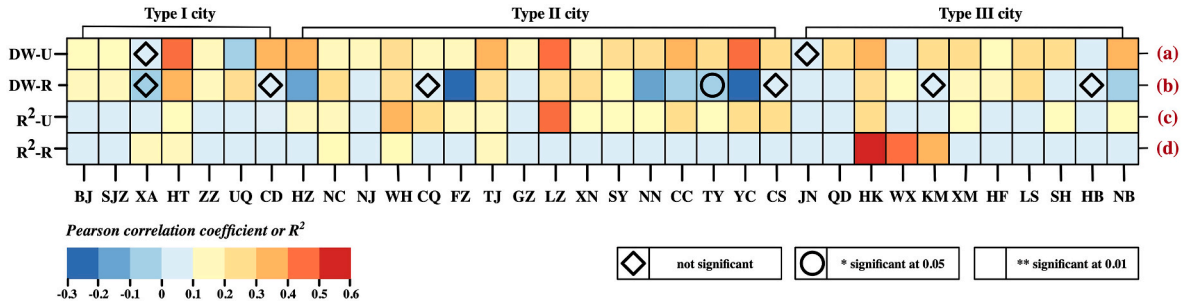


Fig. 7. Pearson correlation coefficient between DW and LST in urban (a) and rural areas (b); R-square of the fitted third-order polynomial function between DW and LST in urban (c) and rural areas (d).

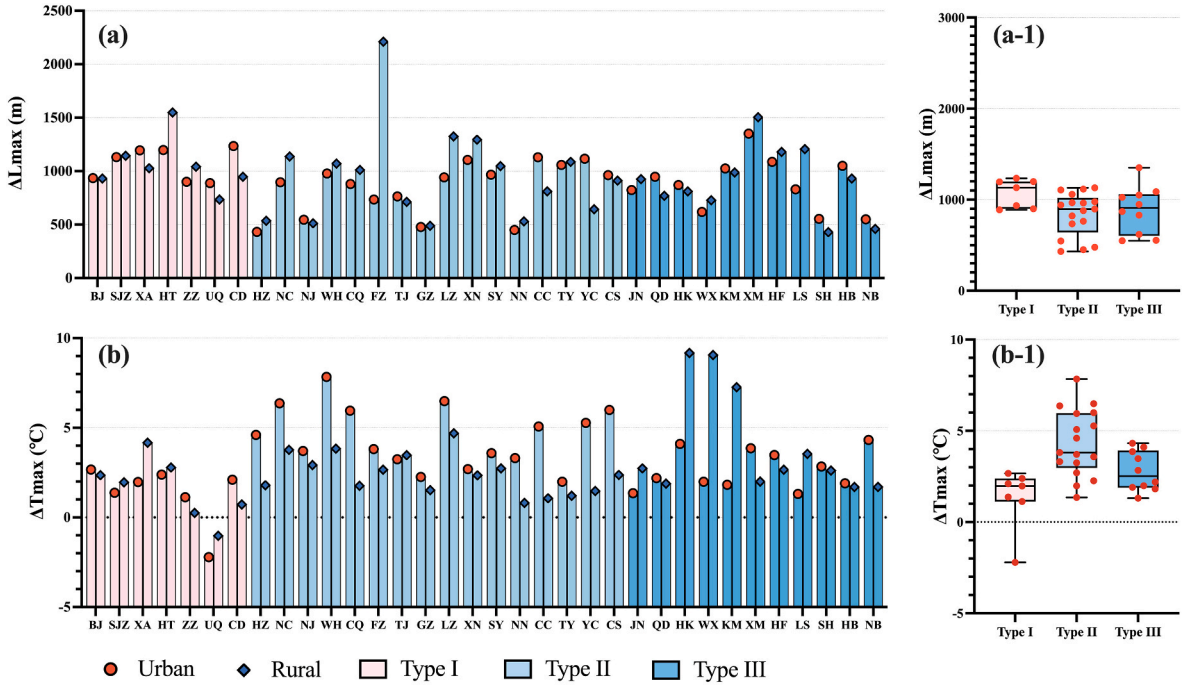


Fig. 8. ΔL_{max} (a) and ΔT_{max} (b) for the 34 cities in urban and rural areas; Box plots of ΔL_{max} (a-1) and ΔT_{max} (b-1) across different city-water layout types in urban areas.

Table 1
Classification of waterbodies (Source: Authors).

Categories	Classes	Width or area
River	Small river	width ≤ 100 m
	Medium river	100 m > width ≤ 500 m
	Large river	500 m > width
Lake	Small lake	area ≤ 100 ha
	Medium lake	100 ha < area ≤ 500 ha
	Large lake	500 ha > area
Ocean	Ocean	NA

The decrease in ΔT_{max} in most cities also confirms this insight (Fig. 8b), as the median ΔT_{max} in Type II cities decreases from 3.81 °C (urban) to 2.34 °C (rural), and the median ΔT_{max} in Type I cities decreases from 1.98 °C (urban) to 1.96 °C (rural). In rural areas, there are more green spaces and less built-up surfaces. The cells near waterbodies tend to have a lower LST, which leads to smaller temperature differences (Fig. 11). This reduces the intensity of air exchanges between waterbodies and their surrounding areas.

However, the waterbody coverage still impacts its cooling effect, as WP has a significant positive relationship with ΔTmax both in urban and rural areas, although the correlation decreases from 0.629** (urban) to 0.482** (rural). This shows that the larger percentage of waterbodies, the stronger the cooling effect.

4. Discussion and limitations

4.1. The factors influencing the cooling effects of waterbodies across different types of cities

The varying cooling effects of waterbodies in different types of cities can be explained by the waterbodies' characteristics and the surrouding urban spatial form. Large waterbodies have a stronger cooling effect than smaller ones, as has been identified in several studies (Zhu et al., 2011; Gunawardena et al., 2017). Fig. 6a shows that a city tends to have a higher WP_U when a large river flows through it. Without large rivers and just small lakes dispersed within the city, WP_U tends to be lower. Thus, Type II and Type III cities, with a higher WP_U, have a bigger ΔT_{max} as compared to Type I cities. Moreover, in Type II cities, rivers flow through the city, and the city center is always adjacent or close to waterbodies. As the city center has always a higher LST, this can produce a big temperature difference among land surface and waterbody surface. The hot and dry air in the city center quickly heats the cooler and humid air from the waterbodies and reduces their cooling distance (Ampatzidis

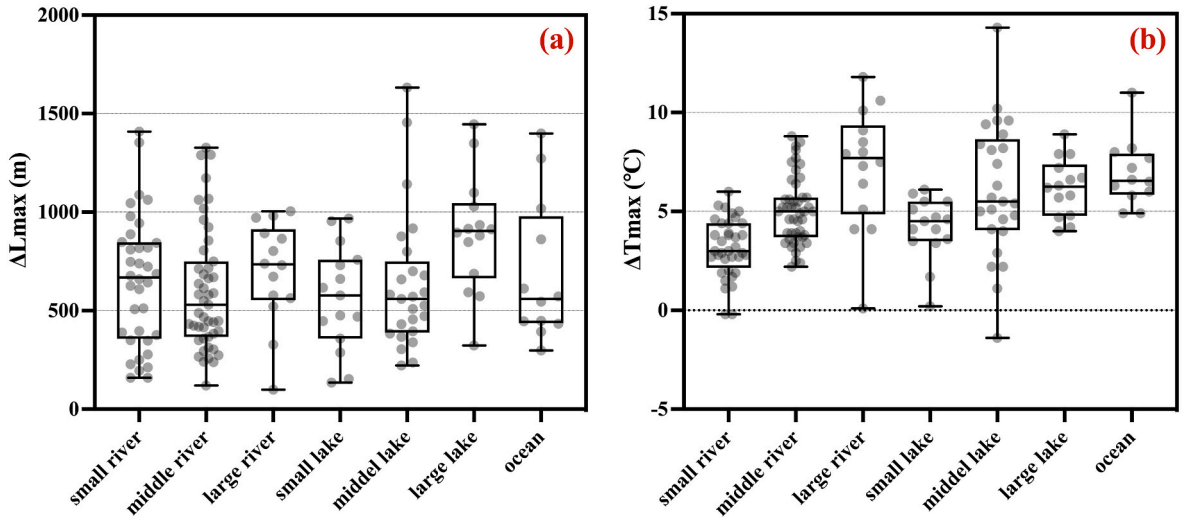


Fig. 9. Box plots of ΔL_{max} (a) and ΔT_{max} (b) across different classes of waterbodies.

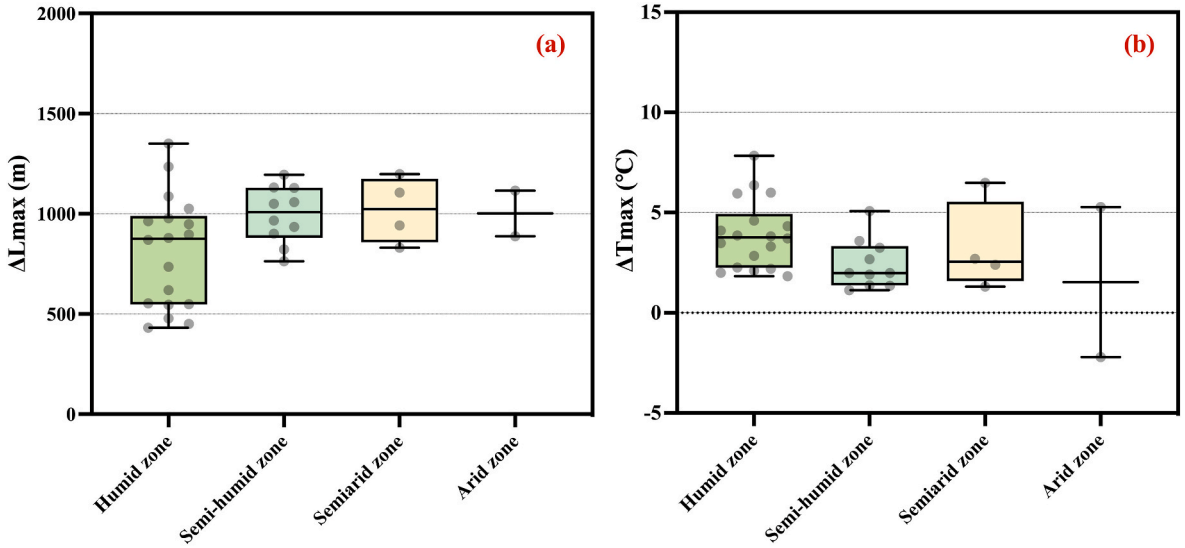


Fig. 10. Box plots of ΔL_{max} (a) and ΔT_{max} (b) across different dry-wet climate regions for the 34 cities.

and Kershaw, 2020). High-rise buildings along the river can also shut off the cooling effect of the rivers and produce a smaller cooling distance (Hathway and Sharples, 2012).

4.2. The warming effect of waterbodies

Waterbodies do not always have a cooling effect on their surrounding areas. They may act as a warm island, as in Urumqi (UQ), where DW displays a significant negative correlation with LST (−0.072**). LST displays a decreasing trend with increasing distance from waterbodies, which act as a warm islands in the city. UQ is located in the arid zone. There are few waterbodies dispersed within the city, and most are small interior lakes. Water rarely flows, with little energy exchanges with surrounding areas. This makes small waterbodies easily heated by solar radiation and urban anthropogenic heat. Shallower static waterbodies reach peak surface temperatures sooner than others, as identified in earlier studies (Oke, 2002; Gunawardena et al., 2017).

It should also be noted that stronger cooling effects almost always happen around noontime, when waterbodies are slowly heated by solar radiation and are cooler than land surfaces, therefore cooling surrounding areas. After noontime and especially at nighttime, as solar radiation gradually decreases, the temperature of the water body decreases more slowly than the surrounding areas, producing a warming effect on the city (Moyer and Hawkins, 2017; Jacobs et al., 2020; Ampatzidis and Kershaw, 2020). Moreover, humidity can also increase the heat capacity and heat accumulation of the air, thus reducing the efficiency of heat exchanges between the human body and the air. This can produce an uncomfortable thermal environment (Lai et al., 2019).

4.3. Limitations and future work

In this study, LST was retrieved from RS images acquired around summer noontime, which is a limitation. Some studies, using air temperature or satellite sensors to explore the thermal effect of waterbodies at other times, have contrary findings. For example, Theeuwes et al. (2013) and Gunawardena et al. (2017) point out that waterbodies have a warming effect during nighttime/winter. Such analyses were not carried out here because of data limitations. The commonly-used free satellite sensors are Landsat and MODIS, which tend to fly over China in the morning or around noontime. Although MODIS has a sensor that can acquire LST at nighttime, it cannot be used in detailed spatial analyses because its thermal band has a spatial resolution of 1000 m. Using

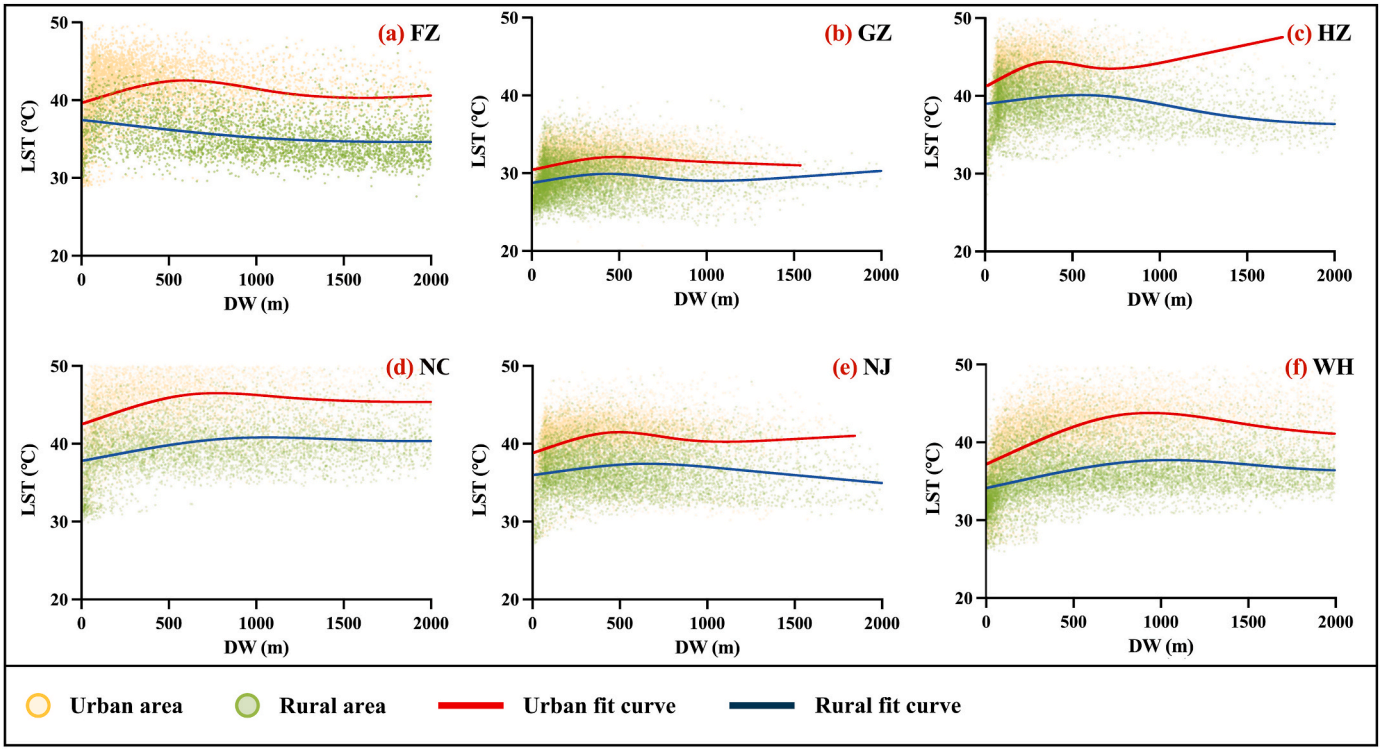


Fig. 11. Scatter plots between LST and DW in urban and rural areas (a-f are the examples of different cities).

data-fusion methods with various sensors to produce high-resolution spatiotemporal datasets may be an area for further research (Gao et al., 2021), which would allow comparing waterbodies' cooling or warming effects at different periods. Also, LST was resampled from a 30 m to a 300 m spatial resolution. Therefore, narrow rivers or small waterbodies were excluded here. However, these waterbodies may have an active role in the urban thermal environment because of their large numbers (Gunawardena et al., 2017). Other studies have also pointed out that urban configuration and spatial form have an impact on the urban thermal environment and the cooling effect of waterbodies (Liu et al., 2019; Zhou et al., 2019). This is also an area for further research, as the presence of green spaces and various building configurations can also affect the observed cooling effect and the maximum cooling distance.

5. Conclusions

We have compared the cooling effects of waterbodies in 34 Chinese megacities located in different dry-wet climate regions. Different water body distributions have led to a classification of city-water layouts: waterbodies dispersed within the city (Type I), waterbodies flowing through the city (Type II), and waterbodies on one side of the city (Type III).

Waterbodies in the three types of city-water layout display different thermal effects. In most cities, waterbodies have a strong cooling effect. Within urban areas, ΔL_{max} ranges from 431 m to 1350 m, and ΔT_{max} ranges from - 2.21 °C to 7.83 °C. The cooling effects of waterbodies are weaker in rural areas. The cooling effect is also affected by WP, both in urban and rural areas. WP has a significant negative relationship with ΔL_{max}, but a significant positive relationship with ΔT_{max}. The larger the area share of waterbodies, the larger ΔT_{max}, but the shorter ΔL_{max}. However, not all waterbodies display a cooling effect, as a warming effect has been observed in the desert city of Urumqi. The cooling effect of waterbodies is also influenced by their size, location and background climate regions. Waterbodies in the humid zone tend to have a bigger ΔT_{max} and a shorter ΔL_{max} than in the arid zone. These findings help better understand the thermal effects of waterbodies and use different planning methods to improve urban resilience and mitigate the SUHI in different cities.

Credit author statement

Zhi Cai: Writing – original draft, Resources, Methodology; **Jean-Michel Guldmann**: Writing – review & editing, Methodology; **Yan Tang**: Writing – review, Project adminstration, Supervision; **Guifeng Han**: Validation and review.

Declaration of competing interest

The authors declare that they have no known competing financial interests or personal relationships that could have appeared to influence the work reported in this paper.

Acknowledgments

This work was supported by the National Natural Science Foundation of China (No. 51978363, No. 51978091), Beijing Social Science Foundation (Grant No. 19GLB034), Beijing Key Laboratory of Spatial Development for Capital Region (Grant No. CLAB202009).

Appendix A. Supplementary data

Supplementary data to this article can be found online at https://doi.org/10.1016/j.jenvman.2022.116263.

References

Adams, M.P., Smith, P.L., 2014. A systematic approach to model the influence of the type and density of vegetation cover on urban heat using remote sensing. Landsc. Urban Plann. 132, 47–54.

Alvarez-Mendoza, C.I., Teodoro, A., Freitas, A., Fonseca, J., 2020. Spatial estimation of chronic respiratory diseases based on machine learning procedures—an approach

using remote sensing data and environmental variables in quito, Ecuador. Appl. Geogr. 123, 102273.
Almeida, C.R.D., Teodoro, A.C., Gonçalves, A., 2021. Study of the urban heat island (UHI) using remote sensing data/techniques: a systematic review. Environments 8 (10), 105.
Ampatzidis, P., Kershaw, T., 2020. A Review of the Impact of Blue Space on the Urban Microclimate. Science of The Total Environment, 139068.
Bande, L., Manadhar, P., Marpu, P., 2019. Definition of local climate zones in relation to ENVI-met and site data in the city of Al ALAIN, UAE. Sustain. City XIII 238, 209.
Cai, Z., Han, G., Chen, M., 2018. Do waterbodies play an important role in the relationship between urban form and land surface temperature? Sustain. Cities Soc. 39, 487–498.
Cai, Z., Tang, Y., Chen, K., Han, G., 2019. Assessing the heat vulnerability of different local climate zones in the old areas of a Chinese megacity. Sustainability 11 (7), 2032.
Cai, Z., Tang, Y., Zhan, Q., 2021. A cooled city? Comparing human activity changes on the impact of urban thermal environment before and after city-wide lockdown. Build. Environ. 195, 107729.
Chun, B., Guldmann, J.M., 2014. Spatial statistical analysis and simulation of the urban heat island in high-density central cities. Landsc. Urban Plann. 125, 76–88.
Chun, B., Guldmann, J.M., 2018. Impact of greening on the urban heat island: seasonal variations and mitigation strategies. Comput. Environ. Urban Syst. 71, 165–176.
Dai, Z., Guldmann, J.M., Hu, Y., 2019. Thermal impacts of greenery, water, and impervious structures in Beijing's Olympic area: a spatial regression approach. Ecol. Indicat. 97, 77–88.
Du, H., Song, X., Jiang, H., Kan, Z., Wang, Z., Cai, Y., 2016. Research on the cooling island effects of water body: a case study of Shanghai, China. Ecol. Indicat. 67, 31–38.
Gao, H., Zhu, X., Guan, Q., Yang, X., Yao, Y., Zeng, W., Peng, X., 2021. cuFSDAF: an enhanced flexible spatiotemporal data fusion algorithm parallelized using graphics processing units. IEEE Trans. Geosci. Rem. Sens. 60, 1–16.
Ghosh, S., Das, A., 2018. Modelling urban cooling island impact of green space and waterbodies on surface urban heat island in a continuously developing urban area. Model. Earth Syst. Environ. 4 (2), 501–515.
Gunawardena, K.R., Wells, M.J., Kershaw, T., 2017. Utilising green and bluespace to mitigate urban heat island intensity. Sci. Total Environ. 584, 1040–1055.
Han, G.F., Cai, Z., Xie, Y.S., Zeng, W., 2016. Correlation between urban construction and urban heat island: a case study in Kaizhou District, Chongqing. J. Civ. Arch. Env. Eng 38, 138–147 (In Chinese).
Hathway, E.A., Sharples, S., 2012. The interaction of rivers and urban form in mitigating the Urban Heat Island effect: a UK case study. Build. Environ. 58, 14–22.
Jacobs, C., Klok, L., Bruse, M., Cortesão, J., Lenzholzer, S., Kluck, J., 2020. Are urban waterbodies really cooling? Urban Clim. 32, 100607.
Jaganmohan, M., Knapp, S., Buchmann, C.M., Schwarz, N., 2016. The bigger, the better? The influence of urban green space design on cooling effects for residential areas. J. Environ. Qual. 45 (1), 134–145.
Jiang, Y., Huang, J., Shi, T., Wang, H., 2021. Interaction of urban rivers and green space morphology to mitigate the urban heat island effect: case-based comparative analysis. Int. J. Environ. Res. Publ. Health 18 (21), 11404.
Klok, E.L., Kluck, J.J., 2018. Reasons to adapt to urban heat (in The Netherlands). Urban Clim. 23, 342–351.
Lai, D., Liu, W., Gan, T., Liu, K., Chen, Q., 2019. A review of mitigating strategies to improve the thermal environment and thermal comfort in urban outdoor spaces. Sci. Total Environ. 661, 337–353.
Lin, W., Yu, T., Chang, X., Wu, W., Zhang, Y., 2015. Calculating cooling extents of green parks using remote sensing: method and test. Landsc. Urban Plann. 134, 66–75.
Lin, Y., Wang, Z., Jim, C.Y., Li, J., Deng, J., Liu, J., 2020. Water as an urban heat sink: blue infrastructure alleviates urban heat island effect in megacity agglomeration. J. Clean. Prod., 121411
Lindsey, R., 2014. How Much Will Earth Warm if Carbon Dioxide Doubles Preindustrial Levels, vol. 24. NOAA Climate. gov, January.
Liu, H., Zhan, Q., Gao, S., Yang, C., 2019. Seasonal variation of the spatially non-stationary association between land surface temperature and urban landscape. Rem. Sens. 11 (9), 1016.
Manoli, G., Fatichi, S., Schläpfer, M., Yu, K., Crowther, T.W., Meili, N., et al., 2019. Magnitude of urban heat islands largely explained by climate and population. Nature 573 (7772), 55–60.
Masoudi, M., Tan, P.Y., Liew, S.C., 2019. Multi-city comparison of the relationships between spatial pattern and cooling effect of urban green spaces in four major Asian cities. Ecol. Indicat. 98, 200–213.
Mora, C., Dousset, B., Caldwell, I.R., Powell, F.E., Geronimo, R.C., Bielecki, C.R., et al., 2017. Global risk of deadly heat. Nat. Clim. Change 7 (7), 501–506.
Moyer, A.N., Hawkins, T.W., 2017. River effects on the heat island of a small urban area. Urban Clim. 21, 262–277.
Oke, T.R., 2002. Boundary layer climates. Routledge.
Oke, T.R., Mills, G., Christen, A., Voogt, J.A., 2017. Urban Climates. Cambridge University Press.Oke, T. R (2002). Boundary layer climates. Routledge.
Park, C.Y., Lee, D.K., Asawa, T., Murakami, A., Kim, H.G., Lee, M.K., Lee, H.S., 2019. Influence of urban form on the cooling effect of a small urban river. Landsc. Urban Plann. 183, 26–35.
Qiu, X.Y., Kil, S.H., Park, C., 2021. Impact of local environment on cooling island effect of water body: case study of Changsha, China. Sensor. Mater 33, 3801–3817.
Rydin, Y., Bleahu, A., Davies, M., Dávila, J.D., Friel, S., De Grandis, G., et al., 2012. Shaping cities for health: complexity and the planning of urban environments in the 21st century. Lancet 379 (9831), 2079–2108.
Shen, T., Chow, D.H.C., Darkwa, J., 2013. Simulating the influence of micro- climatic design on mitigating the urban heat island effect in the hangzhou metropolitan area of China. Int. J. Low Carbon Technol. 11 (1), 130–139. https://doi.org/10.1093/ijlct/ctt050.
Sekertekin, A., Bonafoni, S., 2020. Land surface temperature retrieval from Landsat 5, 7, and 8 over rural areas: assessment of different retrieval algorithms and emissivity models and toolbox implementation. Rem. Sens. 12 (2), 294.
Singh, M., Sharston, R., 2022. Quantifying the dualistic nature of urban heat Island effect (UHI) on building energy consumption. Energy Build. 255, 111649.
Sippel, S., Meinshausen, N., Fischer, E.M., Székely, E., Knutti, R., 2020. Climate change now detectable from any single day of weather at global scale. Nat. Clim. Change 10 (1), 35–41.
Song, J., Du, S., Feng, X., Guo, L., 2014. The relationships between landscape compositions and land surface temperature: quantifying their resolution sensitivity with spatial regression models. Landsc. Urban Plann. 123, 145–157.
Steeneveld, G.J., Koopmans, S., Heusinkveld, B.G., Theeuwes, N.E., 2014. Refreshing the role of open water surfaces on mitigating the maximum urban heat island effect. Landsc. Urban Plann. 121, 92–96.
Sun, R., Chen, L., 2012. How can urban waterbodies be designed for climate adaptation? Landsc. Urban Plann. 105 (1–2), 27–33.
Sun, R., Chen, A., Chen, L., Lü, Y., 2012. Cooling effects of wetlands in an urban region: the case of Beijing. Ecol. Indicat. 20, 57–64.
Sun, Y., Gao, C., Li, J., Wang, R., Liu, J., 2019. Quantifying the effects of urban form on land surface temperature in subtropical high-density urban areas using machine learning. Rem. Sens. 11 (8), 959.
Syafii, N.I., Ichinose, M., Kumakura, E., Jusuf, S.K., Chigusa, K., Wong, N.H., 2017. Thermal environment assessment around bodies of water in urban canyons: a scale model study. Sustain. Cities Soc. 34, 79–89.
Theeuwes, N.E., Solcerová, A., Steeneveld, G.J., 2013. Modeling the influence of open water surfaces on the summertime temperature and thermal comfort in the city. J. Geophys. Res. Atmos. 118 (16), 8881–8896.
Tsai, C.W., Young, T., Warren, P.H., Maltby, L., 2017. Riparian thermal conditions across a mixed rural and urban landscape. Appl. Geogr. 87, 106–114.
United Nations, 2019. Department of Economic and Social Affairs, Population Division. United Nations, New York. World Urbanization Prospects: The 2018 Revision (ST/ESA/SER.A/420).
Van Hoof, J., Schellen, L., Soebarto, V., Wong, J.K.W., Kazak, J.K., 2017. Ten questions concerning thermal comfort and ageing. Build. Environ. 120, 123–133.
Wang, Y., Zhan, Q., Ouyang, W., 2019. How to quantify the relationship between spatial distribution of urban waterbodies and land surface temperature? Sci. Total Environ. 671, 1–9.
Wang, Y., Ouyang, W., 2021. Investigating the heterogeneity of water cooling effect for cooler cities. Sustain. Cities Soc. 75, 103281.
Wang, Z.H., Fan, C., Myint, S.W., Wang, C., 2016. Size matters: what are the characteristic source areas for urban planning strategies? PLoS One 11 (11), e0165726.
Wilson, B., 2013. Urban form and residential electricity consumption: evidence from Illinois, USA. Landsc. Urban Plann. 115, 62–71.
Wu, C., Li, J., Wang, C., Song, C., Chen, Y., Finka, M., La Rosa, D., 2019. Understanding the relationship between urban blue infrastructure and land surface temperature. Sci. Total Environ. 694, 133742.
Wu, J., Li, C., Zhang, X., Zhao, Y., Liang, J., Wang, Z., 2020. Seasonal variations and main influencing factors of the water cooling islands effect in Shenzhen. Ecol. Indicat. 117, 106699.
Xu, H., 2007. Extraction of urban built-up land features from Landsat imagery using a thematicoriented index combination technique. Photogramm. Eng. Rem. Sens. 73 (12), 1381–1391.
Xu, H., 2008. A new index for delineating built-up land features in satellite imagery. Int. J. Rem. Sens. 29 (14), 4269–4276.
Xue, Z., Hou, G., Zhang, Z., Lyu, X., Jiang, M., Zou, Y., et al., 2019. Quantifying the cooling-effects of urban and peri-urban wetlands using remote sensing data: case study of cities of Northeast China. Landsc. Urban Plann. 182, 92–100.
Yang, G., Yu, Z., Jørgensen, G., Vejre, H., 2020. How can urban blue-green space be planned for climate adaption in high-latitude cities? A seasonal perspective. Sustain. Cities Soc. 53, 101932.
Yang, J., Yin, P., Sun, J., Wang, B., Zhou, M., Li, M., et al., 2019. Heatwave and mortality in 31 major Chinese cities: definition, vulnerability and implications. Sci. Total Environ. 649, 695–702.
Zhang, W., Zheng, C., Chen, F., 2019. Mapping heat-related health risks of elderly citizens in mountainous area: a case study of Chongqing, China. Sci. Total Environ. 663, 852–866.
Zhao, L., Oppenheimer, M., Zhu, Q., Baldwin, J.W., Ebi, K.L., Bou-Zeid, E., et al., 2018. Interactions between urban heat islands and heat waves. Environ. Res. Lett. 13 (3), 034003.
Zhou, D., Xiao, J., Bonafoni, S., Berger, C., Deilami, K., Zhou, Y., et al., 2019. Satellite remote sensing of surface urban heat islands: progress, challenges, and perspectives. Rem. Sens. 11 (1), 48.
Zhu, C.Y., Li, S.H., Ji, P., Ren, B.B., Li, X.Y., 2011. Effects of the different width of urban green belts on the temperature and humidity. Acta Ecol. Sin. 31 (2), 383–394.